Semiclassical quantization of sawtooth map with inclusion of next leading order and its failure

1996 J. Phys. A: Math. Gen. 29 6087

(http://iopscience.iop.org/0305-4470/29/18/034)

J. Phys. A: Math. Gen. **29** (1996) 6087–6110. Printed in the UK

Semiclassical quantization of sawtooth map with inclusion of next leading order and its failure

Mitsusada M Sano†

Centre for Nonlinear Phenomena and Complex Systems, Université Libre de Bruxelles, Campus Plaine CP 231, Blvd. du Triomphe, B-1050 Bruxelles, Belgium
and
Department of Applied Physics, Tokyo Institute of Technology, Oh-okayama, 2-12-10, Meguro 152, Tokyo, Japan

Received 18 March 1996

Abstract. The semiclassical quantization of sawtooth maps is reconsidered from the viewpoint of the higher-order terms in the asymptotic series. We carry out the semiclassical quantization in the leading and next leading orders. However, we fail in both cases. The reasons are discussed in detail.

1. Introduction

The quantization of chaotic systems is one of the hottest topics in contemporary theoretical physics and is related to various quantum phenomena. The semiclassical theory plays an essential role in such studies. The main problem is: 'how can we construct quantum eigenenergies from information about the corresponding classical dynamics?'. Formally, it can be done by using the Gutzwiller trace formula [1] or the associated zeta function [2] in terms of information on periodic orbits, although there is a convergence problem caused by the exponential proliferation of periodic orbits. This difficulty was solved by Berry and Keating [3], at least to leading order, using a resummation technique with analogy to the Riemann zeta function. Now the major interest is in the higher-order corrections and the resurgence relation in the asymptotic series. The higher-order corrections can be categorized in three classes as follows. (1) Diffraction, which arises in discontinuous systems, e.g. the creeping wave [4] and the edge contribution [5, 6] in billiard systems. (2) Complex stationary points, which describe quantum tunneling paths [11–13]. (3) Higher-order terms in the Taylor series of the action around a (real or complex) stationary point (i.e. nonlinearity in the Jacobi field). The latter can be systematically enumerated [14]. However, in a theoretical sense, it has not yet been fully understood what kinds of phenomena arise from the effects (1)–(3) when the underlying classical dynamics is chaotic.

In the present paper, using a simple model (the quantized sawtooth map), we concentrate on the role of the higher-order contribution in the whole asymptotic expansion. Here we briefly explain the characteristic features of the classical and quantized sawtooth maps. The

† Present address: Department of Fundamental Sciences, Faculty of Integrated Human Studies-FIHS, Kyoto University, Sakyo-ku, Kyoto, 606-01, Japan.

0305-4470/96/186087+24$19.50

classical sawtooth map is an extension of Arnold's cat map, which is defined on the torus $\mathbb{T}^2$ and is given as

$$H = f(p) + g(q) \sum_{n=-\infty}^{+\infty} \delta(t-n). \tag{1}$$

where $f(p)$ and $g(q)$ are

$$f(p) = \tfrac{1}{2}(p-\tfrac{1}{2})^2 \qquad g(q) = -\frac{K}{2}(q-\tfrac{1}{2})^2 \qquad q, p \in [0,1). \tag{2}$$

Here K is real, and $f(p)$ and $g(q)$ obey the periodic boundary conditions $f(p) = f(p+1)$, $g(q) = g(q+1)$. The mapping is

$$\begin{aligned} q_{n+1} &= q_n + p_{n+1} - \tfrac{1}{2} - w_q^{(n)} \\ p_{n+1} &= p_n + K(q_n - \tfrac{1}{2}) - w_p^{(n)} \end{aligned} \tag{3}$$

where $w_q^{(n)}, w_p^{(n)} \in \mathbb{Z}$ are the winding numbers for the q and p coordinates, respectively. Arnold's cat map is defined for $K =$ integer. For convenience, we call the case $K \neq$ integer the *non-cat sawtooth map*. The major difference between Arnold's cat map and the non-cat sawtooth map is the latter's discontinuity property. For Arnold's cat map, the discontinuity is cancelled by the modulo operation. Thanks to this property, its classical and quantum dynamics have been extensively investigated. For instance, the ergodic property [21, 22], the distribution of periodic orbits [17, 23], and the semiclassical quantization [15, 16] are all well known. Note that semiclassical theory is exact for the quantized Arnold's cat map (i.e. all higher-order terms vanish), and it displays the number-theoretic level degeneracies [15, 16]. However, for the non-cat sawtooth map, the extension is regarded as a discontinuous perturbation of Arnold's cat map. Then the situation is very different from the case of a smooth perturbation [19, 20]. Since the modulo operation cannot remove the discontinuity in this case, this discontinuous extension induces bifurcation of the trajectories [17] and recovery of the level repulsion [18] for the quantum counterpart. The discontinuity of the dynamics also induces a diffraction effect analogous to the billiard problem. In this paper we explicitly evaluate the diffraction effect and elucidate the relation between the higher-order terms in $\overline{h}$ and the bifurcation of periodic orbits.

The organization of the remainder of this paper is as follows. In section 2, we first carry out the leading-order semiclassical quantization by using the Smilansky zeta function and show its failure. In section 3, using the Fourier transformation of the trace of the powers of the Floquet operator, we examine the effect of the bifurcation of the periodic orbits. In section 4, we evaluate the diffractive contribution and add it to the semiclassical quantization. In section 5, we summarize our results and give our conclusion.

2. Semiclassical quantization to leading order

First we consider the behaviour of the bifurcation of the periodic orbits. For enumeration of the periodic orbits, we used the symbolic dynamics derived by Bird and Vivaldi [17]. In figures 1 and 2, the periodic orbits with period up to 6 for $K = 1.0$ and 1.3 are depicted. For $K = 1.0$ (in general, $K =$ integer), the periodic orbits form a lattice structure. In contrast, for $K =$ non-integer, the periodic orbits are rearranged and bifurcated. In figure 3, the occurrence of the bifurcation for the short periodic orbits are depicted. The vertical axis represents the number of prime periodic orbits up to period 5. The horizontal axis is the perturbation parameter K. The discontinuous steps correspond to the bifurcation of the periodic orbits. The remarkable feature is that the figure looks like a devil's staircase. This is

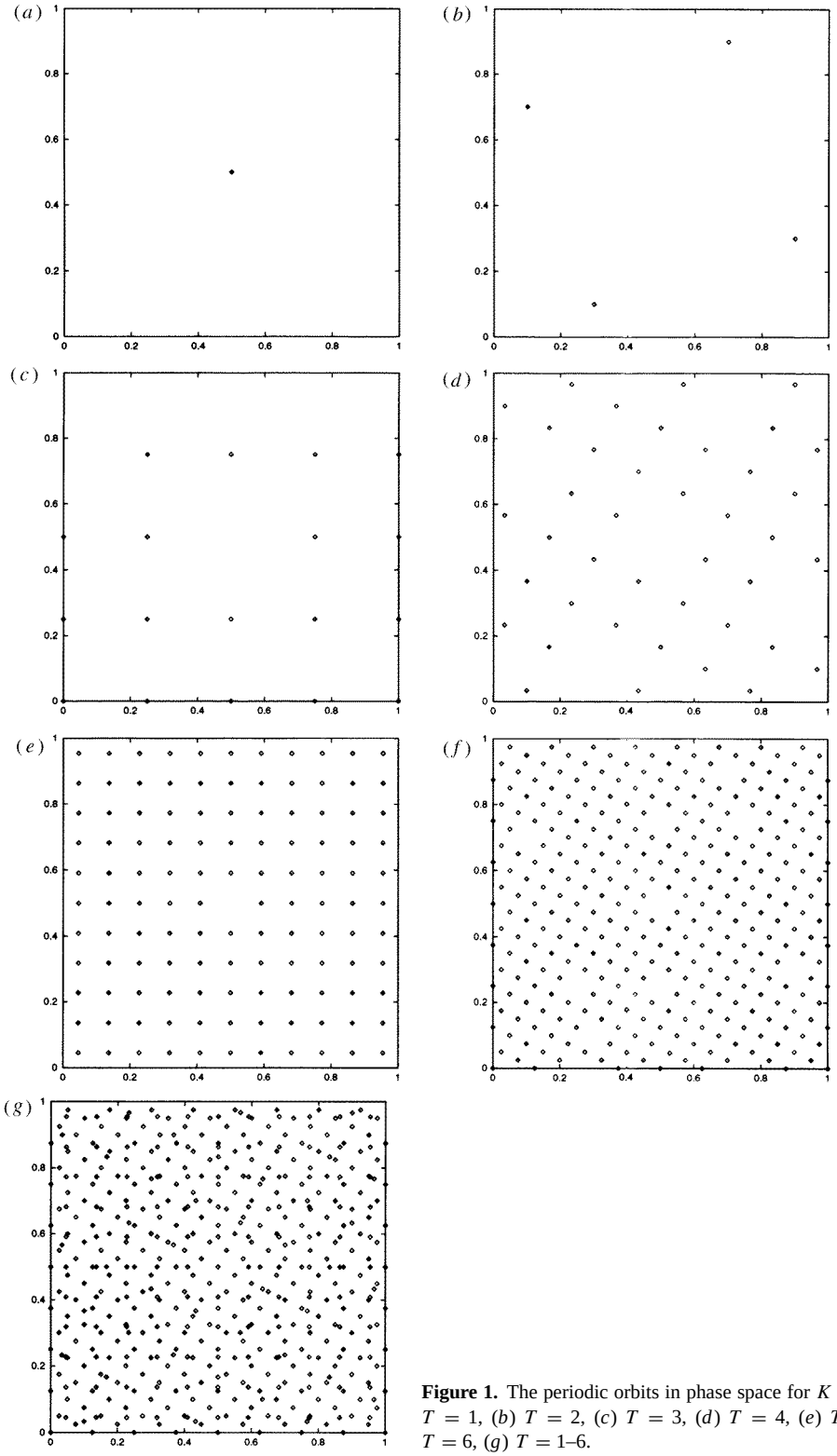

Figure 1. The periodic orbits in phase space for $K = 1.0$. (*a*) $T = 1$, (*b*) $T = 2$, (*c*) $T = 3$, (*d*) $T = 4$, (*e*) $T = 5$, (*f*) $T = 6$, (*g*) $T = 1$–6.

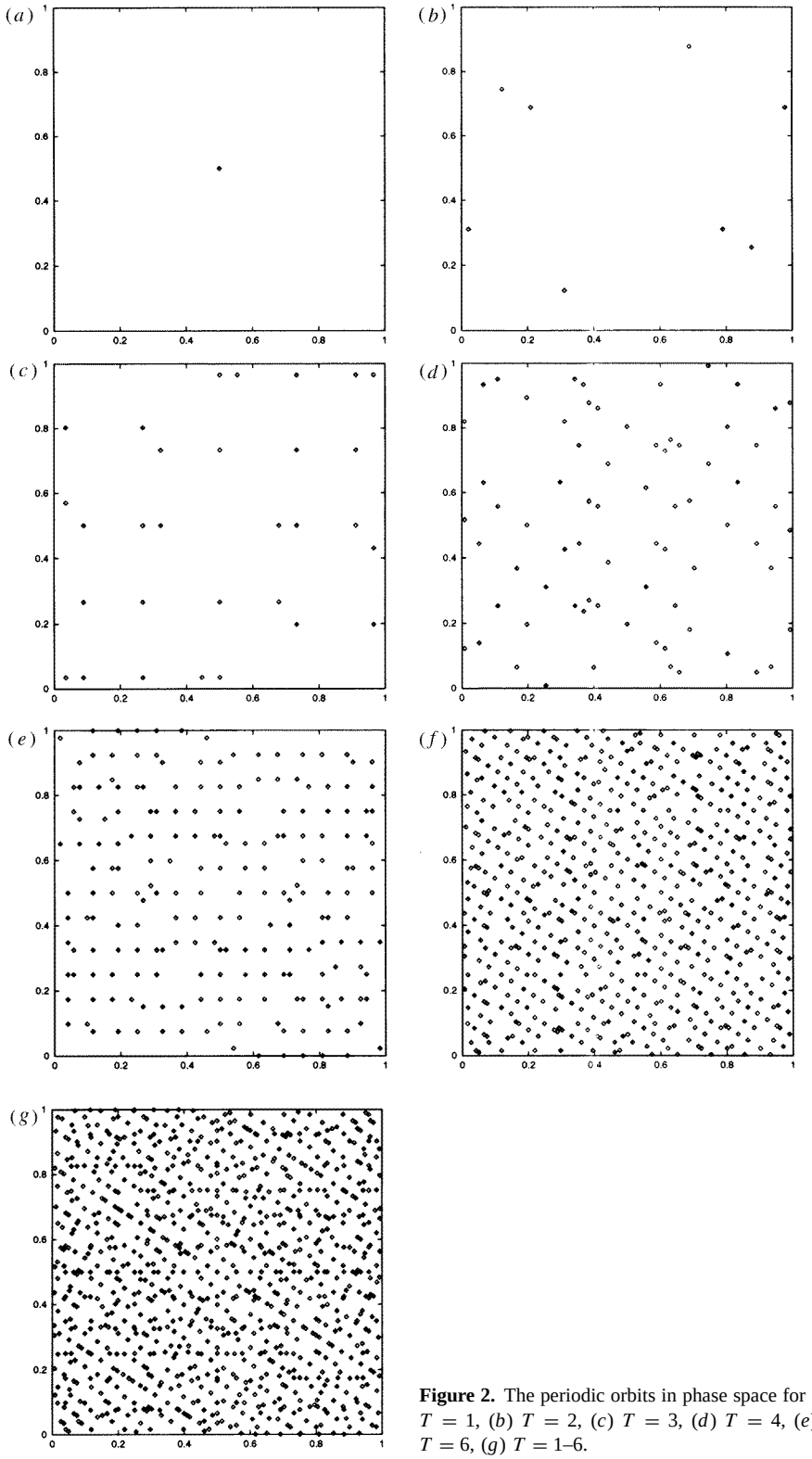

Figure 2. The periodic orbits in phase space for $K = 1.3$. (*a*) $T = 1$, (*b*) $T = 2$, (*c*) $T = 3$, (*d*) $T = 4$, (*e*) $T = 5$, (*f*) $T = 6$, (*g*) $T = 1$–6.

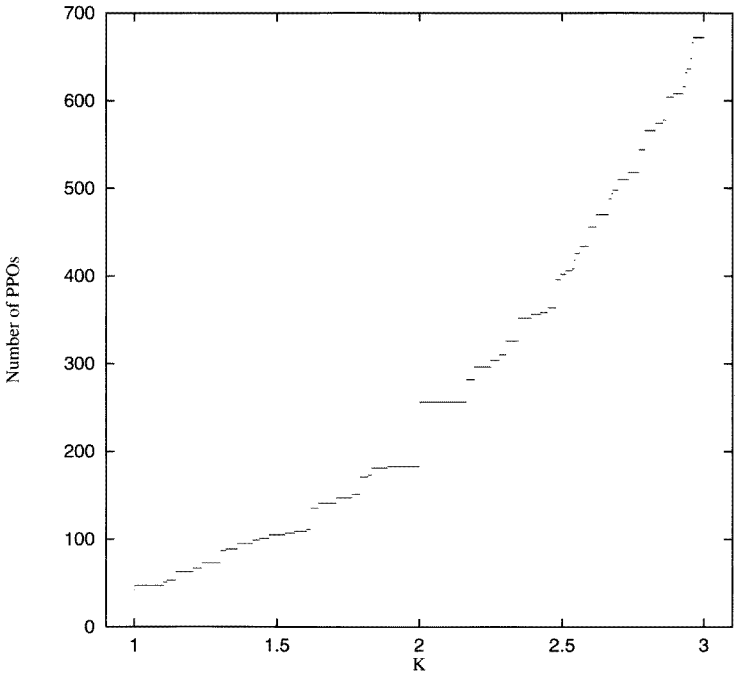

Figure 3. The bifurcation diagram. The vertical axis is the number of prime periodic orbits (PPOs) up to period 5. The horizontal axis is the perturbation parameter K.

a common feature of discontinuous hyperbolic systems, such as hyperbolic billiard systems [7]. The similarity between the sawtooth maps and dispersing billiards was mentioned by Chernov [24]. Without giving a rigorous statement, we expect that a plot of the system parameter K versus the topological entropy would really be a devil's staircase. This drastic behaviour causes a problem in the quantum counter part as we will see later.

The quantum dynamics is governed by the time evolution operator $\hat{U}$ (Floquet operator):

$$\psi(q;t+1) = \hat{U}\psi(q;t) \tag{4}$$

where

$$\hat{U} = \exp\left(-\frac{\mathrm{i}}{\overline{h}} f(\hat{p})\right) \exp\left(-\frac{\mathrm{i}}{\overline{h}} g(\hat{q})\right) \tag{5}$$

and $\hat{p}$ and $\hat{q}$ are momentum and position operators. The eigenvalue problem consists in solving the following equation:

$$\hat{U}\psi_n = \mathrm{e}^{\mathrm{i}\omega_n}\psi_n. \tag{6}$$

Due to the compactness of phase space, the uncertainty relation for the quantum map is given as

$$\frac{1}{2\pi\overline{h}} = N \tag{7}$$

where N is the number of lattice points. The matrix size of the time-evolution operator is just N. By using the Fourier basis, the matrix elements of the quantum time-evolution operator are given as

$$\langle n|\hat{U}|m\rangle = (-1)^{n-m}\frac{\mathrm{e}^{-\frac{\mathrm{i}\pi}{4}}}{\sqrt{N}} \exp\left[\frac{\mathrm{i}\pi}{N} K m^2\right] \exp\left[\frac{\mathrm{i}\pi}{N}(n-m)^2\right]. \tag{8}$$

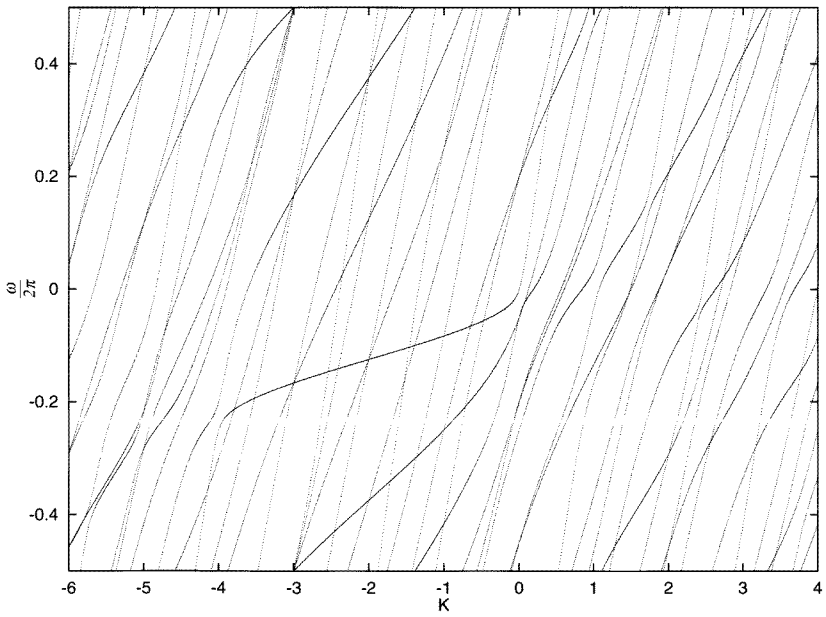

Figure 4. Parametric motion of the eigenangles versus K for $N = 10$.

Here $-\frac{N}{2} \leqslant n, m \leqslant \frac{N}{2} - 1$. Because of the symmetry of the map, the boundary condition is different for even or odd N, namely

$$\begin{aligned} &N = \text{odd: anti-periodic boundary condition } \psi(q+1) = -\psi(q) \\ &N = \text{even: periodic boundary condition } \psi(q+1) = \psi(q). \end{aligned} \tag{9}$$

In this paper, we mainly set $N =$ even. Here we note that the general sawtooth map defined in equations (1)–(3) does not satisfy the quantizability condition, as mentioned in [15].

In figure 4, the parametric dependence of the eigenangles is depicted for $N = 10$. The behaviour for K between -4.0 and 0.0 is qualitatively different from that outside this interval. This reflects the underlying classical dynamics [regular ($-4 < K < 0$) or chaotic ($K < -4$, $K > 0$)]. As reported in [18], the level repulsion immediately occurs when K is changed away from $K =$ integer. However, the level degeneracies are still observed for $K \neq$ integer. From numerical observation, they occur when K is certain rational value. In figure 5, we depict the level spacing distribution for the quantized sawtooth maps. When we change the system parameter K starting from $K =$ integer, the transition from the singular distribution to the Wigner distribution is clearly seen.

To evaluate the eigenangles semiclassically, we use the zeta function formalism. The Selberg-type zeta function for the quantum kicked system was derived by Smilansky [25]. The spectral determinant for $\hat{U}$ is given as

$$P(z) = \det(z - \hat{U}) = \sum_{n=0}^{N} a_n z^n = 0 \tag{10}$$

where $z = \mathrm{e}^{\mathrm{i}\omega}$. Because of the finite dimension of $\hat{U}$, $P(z)$ is a finite series. The coefficients a_k for $k = 1, \ldots, N$ satisfy the Newton relation [25],

$$a_{N-k} = -\frac{1}{k} \sum_{n=1}^{k} a_{N-k+n} \operatorname{Tr}(\hat{U}^n). \tag{11}$$

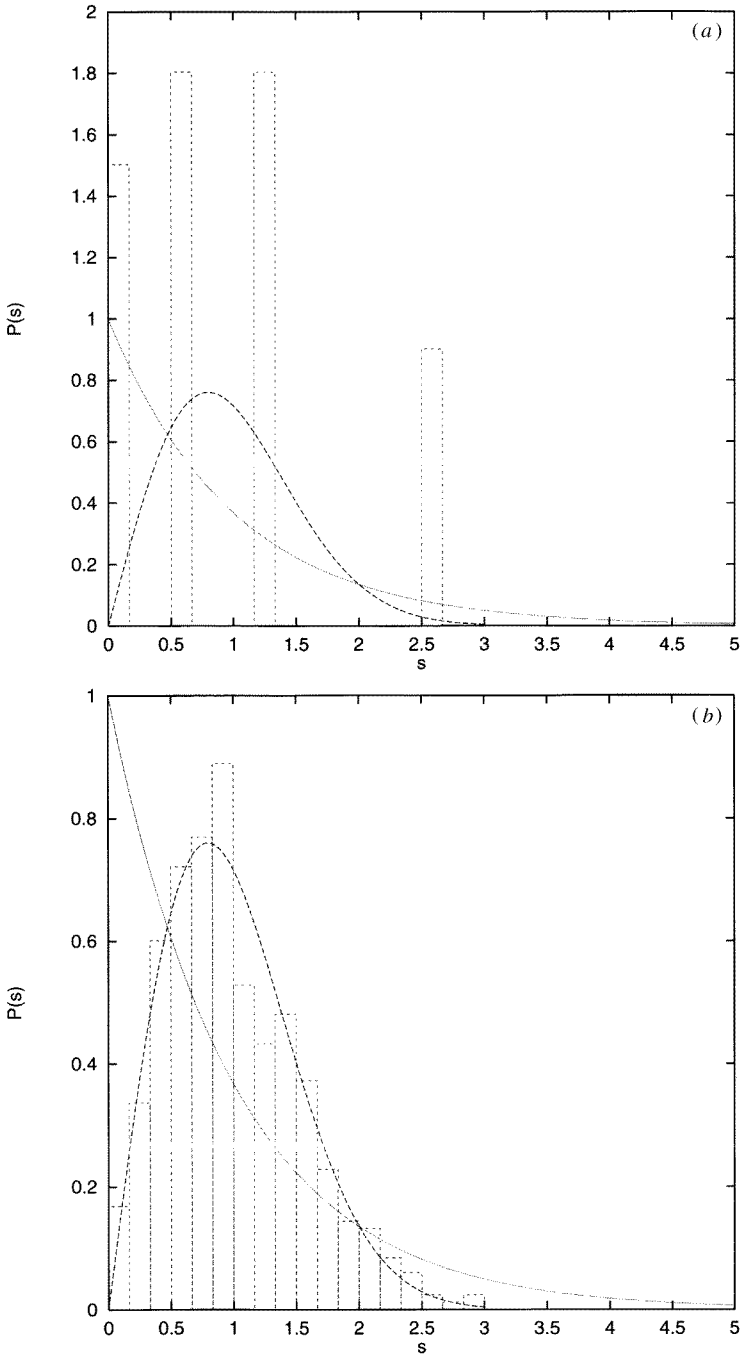

Figure 5. Distributions of the level spacings. (*a*) $K = 1.0$, (*b*) $K = 1.05$, (*c*) $K = 1.3$. The matrix size is $N = 1/2\pi\bar{h} = 500$. The full and broken curves represent the Poisson distribution and the Wigner distribution, respectively.

To investigate the spectral properties, it is convenient to consider the following zeta function:

$$Z(\omega) = \mathrm{e}^{-\mathrm{i}(\Theta+N\omega)/2} P(\mathrm{e}^{\mathrm{i}\omega}) \tag{12}$$

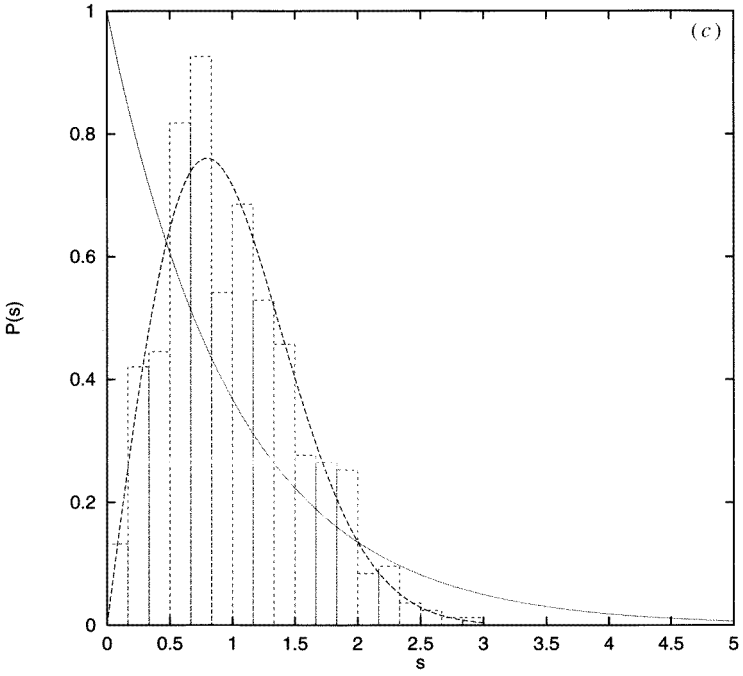

Figure 5. (Continued)

where

$$e^{i\Theta} = e^{i[(\sum_{j=1}^{N}\omega_j)-N\pi]} = \det(-\hat{U}). \tag{13}$$

We can obtain this formula from the analogy with the derivation of the Riemann–Siegel look-alike formula [25]. We note here that for real ω, this zeta function $Z(\omega)$ crosses the real axis and that a_k is related to a_{N-k} (self-inversive property):

$$a_k = a^*_{N-k}e^{i\Theta}. \tag{14}$$

One can show that the trace of integer powers of $\hat{U}$ is given as [26]

$$\mathrm{Tr}^{sc}(\hat{U}^T) = i^n \sum_{po,n=T_{po}r} \frac{T_{po}}{\sqrt{|\det(M^r_{po}-I)|}} \exp\left[\frac{i}{\hbar}S_{po} - \frac{i\pi\nu_{po}}{2}\right] \tag{15}$$

where the action S_{po} is given by

$$S_{po} = \sum_{i=0}^{n-1}\{-(f(p_{po,i})+g(q_{po,i})) + p_{po,i+1}(q_{po,i+1}-q_{po,i}) - w^{(i)}_{po,p}q_{po,i} + w^{(i-1)}_{po,q}p_{po,i}\} \tag{16}$$

and ν_{po} is the Maslov index of the periodic orbit with the index po, and r is the repetition of the periodic orbit. Since we may expect $\Theta \to 0$ in the semiclassical approximation as $\hbar \to 0$, then the zeta function $Z(\omega)$ would be approximated well by $Z_{sc}(\omega)$ defined as follows [25]:

$$Z_{sc}(\omega) = \sum_{l=0}^{[N/2]-\varepsilon_N} [A^*_{N-l}e^{i(l-N/2)\omega} + A_{N-l}e^{-i(l-N/2)\omega}] + \tfrac{1}{2}\varepsilon_N(A_{N/2}+A^*_{N/2}) \tag{17}$$

where

$$\varepsilon_N = \begin{cases} 1 & \text{for even } N \\ 0 & \text{for odd } N \end{cases} \tag{18}$$

and

$$A_k = -\frac{1}{k}\sum_{n=1}^{k} A_{N-k+n}\,\mathrm{Tr}^{\mathrm{sc}}(\hat{U}^n). \tag{19}$$

Here $[x]$ stands for the integer part of x. However, the accuracy of $Z_{\mathrm{sc}}(\omega)$ holds only in the semiclassical limit ($\overline{h} \to 0$). For a relatively large value of $\overline{h}$, we use the following zeta function for even N:

$$\tilde{Z}_{\mathrm{sc}}(\omega) = \sum_{l=0}^{[N/2]-1} \{\mathrm{e}^{\mathrm{i}\Theta/2} A^*_{N-l} \mathrm{e}^{\mathrm{i}(l-N/2)\omega} + \mathrm{e}^{-\mathrm{i}\Theta/2} A_{N-l} \mathrm{e}^{-\mathrm{i}(l-N/2)\omega}\} + \mathrm{e}^{-\mathrm{i}\Theta/2} A_{N/2} \tag{20}$$

with

$$\mathrm{e}^{\mathrm{i}\Theta} = \frac{A_l}{A^*_{N-l}}. \tag{21}$$

We note here that thanks to the self-inversive property, equation (14), the zeta function (17) or (20) has the analytical bootstrap effect, i.e. the latter terms determine the former terms. This effect was mentioned by Voros [27]. This effect poses a very severe restriction on the semiclassical analysis because we have to enumerate all periodic orbits up to period $[N/2]$. In addition, the mechanism of this effect is presently unknown for quantized chaotic systems, especially deep in the quantum regime.

Table 1. Number of prime periodic orbits for $K = 1$ (cat map) and $K = 1.3$ (Non-cat sawtooth map).

Period	Number for $K = 1$	Number for $K = 1.3$
1	1	1
2	2	4
3	5	10
4	10	18
5	24	40
Total	42	78

We carry out the semiclassical quantization based on the zeta function (20). Our numerical result is limited to the deep quantum regime, i.e. for large $\overline{h}$, because for small $\overline{h}$, we have to consider orbits of larger periods T (i.e. exponential proliferation of the number of the periodic orbits). In fact we set $N = 1/2\pi\overline{h} = 10$. First, we consider the case $K = 1.0$ (cat map). The numbers of prime periodic orbits up to period 5 in table 1 and the exact quantum eigenangles in table 2 are listed for the cases $K = 1.0$ and $K = 1.3$. As we can see, the eigenangles are rational multiples of π [15, 16]. The corresponding zeta function is depicted in figure 6(a). Note that for the cat map $K = 1$, the semiclassical result is exact. For $K \neq 1$, the situation is quite different from the case $K = 1$. The number of prime periodic orbits increases for $K = 1.3$. In figure 6, we depict the parametric dependence of the zeta function for $K = 1$ (cat map), 1.1, 1.2, 1.3, 1.4, 1.5. The farther away K is from an integer, the worse is the agreement between the semiclassical and quantum results. In particular, the semiclassical zeta function does not cross the real zero axis near the level

Table 2. Exact quantum eigenangles: $K = 1$ (cat map) and $K = 1.3$ (Non-cat sawtooth map) for $N = 10$.

ith eigenangle	$\omega/2\pi$ for $K = 1$	$\omega/2\pi$ for $K = 1.3$
$i = 1$	−4.666 666 666 7e-01	−4.455 208 539 4e-01
2	−3.666 666 666 7e-01	−4.523 543 334 7e-01
3	−1.666 666 666 7e-01	−2.893 604 605 8e-01
4	−1.333 333 333 3e-01	−2.209 279 591 4e-01
5	−3.333 333 333 3e-02	−6.768 011 443 6e-02
6	3.333 333 333 3e-02	−5.515 429 762 0e-02
7	1.333 333 333 3e-01	6.005 895 678 8e-02
8	1.666 666 666 7e-01	1.816 401 932 6e-01
9	3.666 666 666 7e-01	2.468 690 916 7e-01
10	4.666 666 666 7e-01	3.174 297 774 7e-01

degeneracies in the regime $K \neq$ integer (see also figure 4). Even the pairs of the eigenangles having relatively large spacing can not been reproduced semiclassically. This implies that the missing semiclassical eigenangles are located away from the real axis of the eigenangle ω, that is, $\omega_n^{(\mathrm{sc})} = \omega_n^{(\mathrm{sc,r})} + \mathrm{i}\eta_n$, where $\omega_n^{(\mathrm{sc,r})}$ and η_n are real (i.e. break-down of the unitarity of $\hat{U}^{(\mathrm{sc})}$). The reason for this failure of the semiclassical quantization will be shown in the next section.

3. Fourier transform of $\mathbf{Tr}(\hat{U}^T)$

To understand the discrepancy between the semiclassical and quantum zeta functions for $K = 1.1 \sim 1.5$ in figure 6, we consider how the classical information is contained in the exact quantum trace. To do so, the Fourier transform of the trace (FTT) is a useful tool. The FTT of $\mathrm{Tr}(\hat{U}^T)$ is defined by

$$A(S; M, n_0, T) \equiv \left| \frac{1}{M} \sum_{j=n_0}^{n_0+M-1} \exp[-2\pi j S] \,\mathrm{Tr}\left(\hat{U}^T \left(\hbar = \frac{1}{2\pi j}\right)\right) \right| \qquad (22)$$

where $0 \leqslant S < 1$. It is obvious that the spectrum has peaks at the corresponding classical actions $S_{po} \bmod 1$. The calculation is carried out for K between 0.0 and 3.0 and results are shown in figure 7. In figure 7(a), which corresponds to $T = 1$, the fixed point $S_{po} = 0$ is real. We can see a new peak around $S_{po} = 0$, $K = 1.5$. As will be explained below, this corresponds to the contribution from the torus boundary to the integral. This contribution becomes comparable with the contribution from real periodic orbits near $K = 2$. In figures 7(b)–(e), which represent the higher periods, similar features are observed. We note here that the number of periodic orbits increases as the period increases. As seen in the FTT for billiard systems [8, 9], the peak distribution in the FTT is uniform for higher periods T and for large K, and the birth of new peaks with changing K is random. This randomness can be explained as follows. Since the periodic orbits are uniformly distributed [28], then the bifurcations of periodic orbits occur everywhere in $\mathbb{T}^2$ for changing K. Thus, the action of the bifurcated periodic orbits is also randomly and uniformly distributed. The relationship between the randomness in the bifurcation process and the randomness in the parametric motion of the eigenangles is not yet understood. As a measure of the convergence of each semiclassical trace with respect to $\hbar$, the $\hbar$-dependence of the relative deviation Δ of the semiclassical trace from the exact trace is depicted in figure 8. For higher periods, the convergence is slower and Δ shows some periodic oscillation. This indicates that some

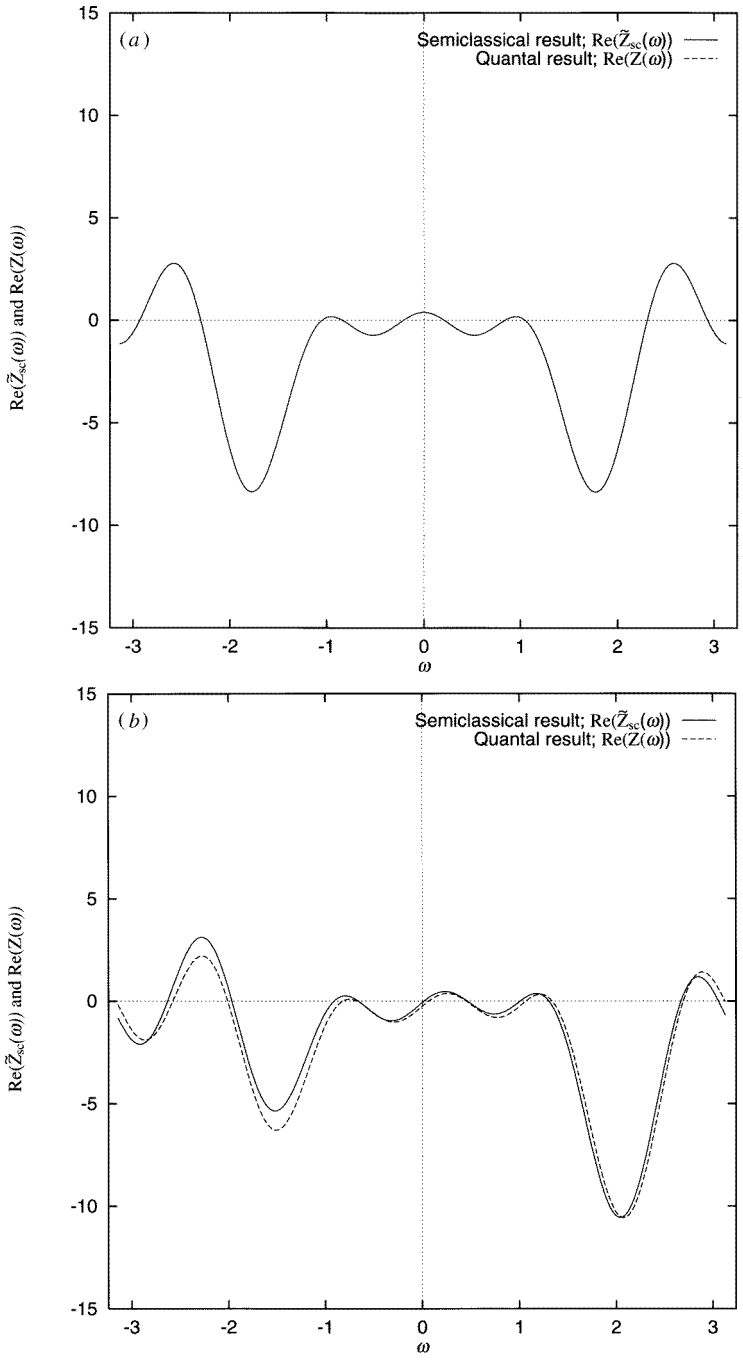

Figure 6. Zeta function : Quantum exact (dotted lines) and semiclassical result ($\mathcal{O}(\bar{h}^0)$, full curves). (*a*) $K = 1.0$ (cat map), (*b*) $K = 1.1$, (*c*) $K = 1.2$, (*d*) $K = 1.3$, (*e*) $K = 1.4$, (*f*) $K = 1.5$. Note that the semiclassical result is exact for $K = 1$.

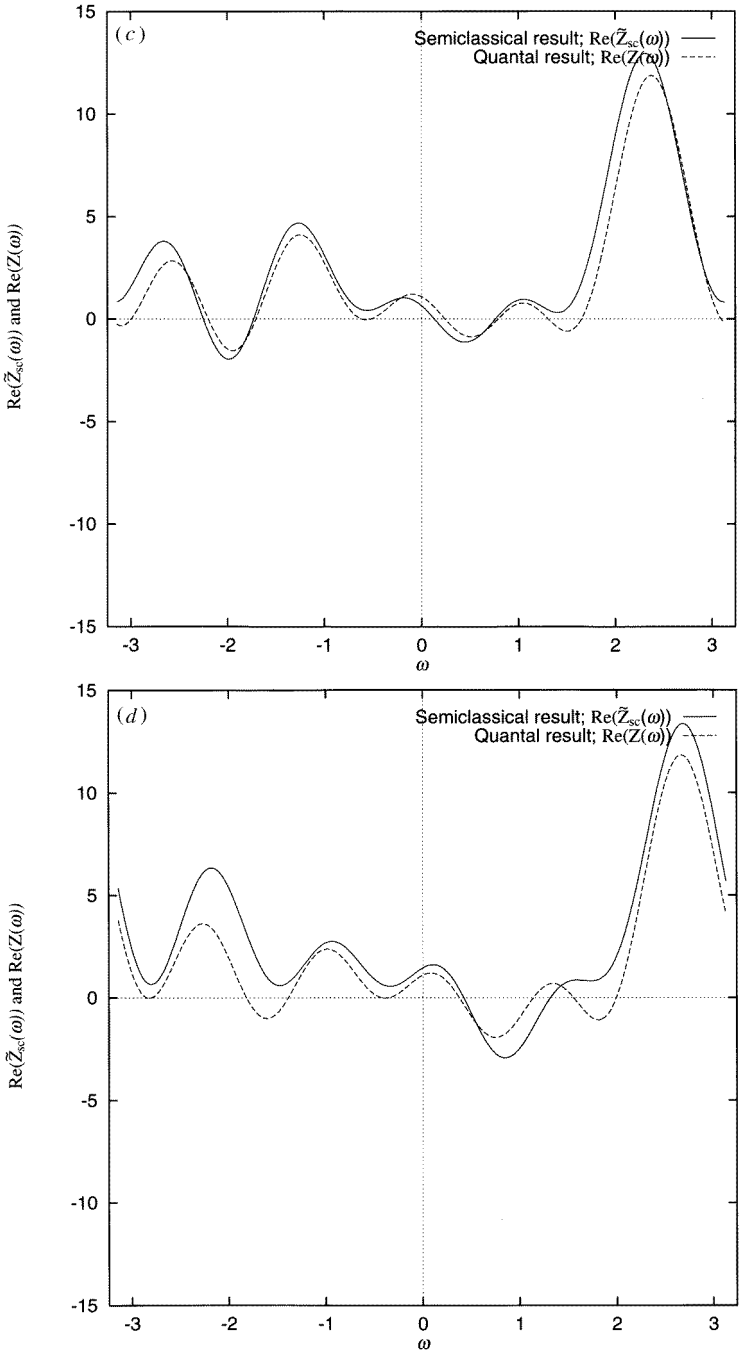

Figure 6. (Continued)

contributions which have non-zero action, are missing in the semiclassical calculation. In the next section, we will carefully examine the asymptotic expansion of $\mathrm{Tr}(\hat{U}^T)$.

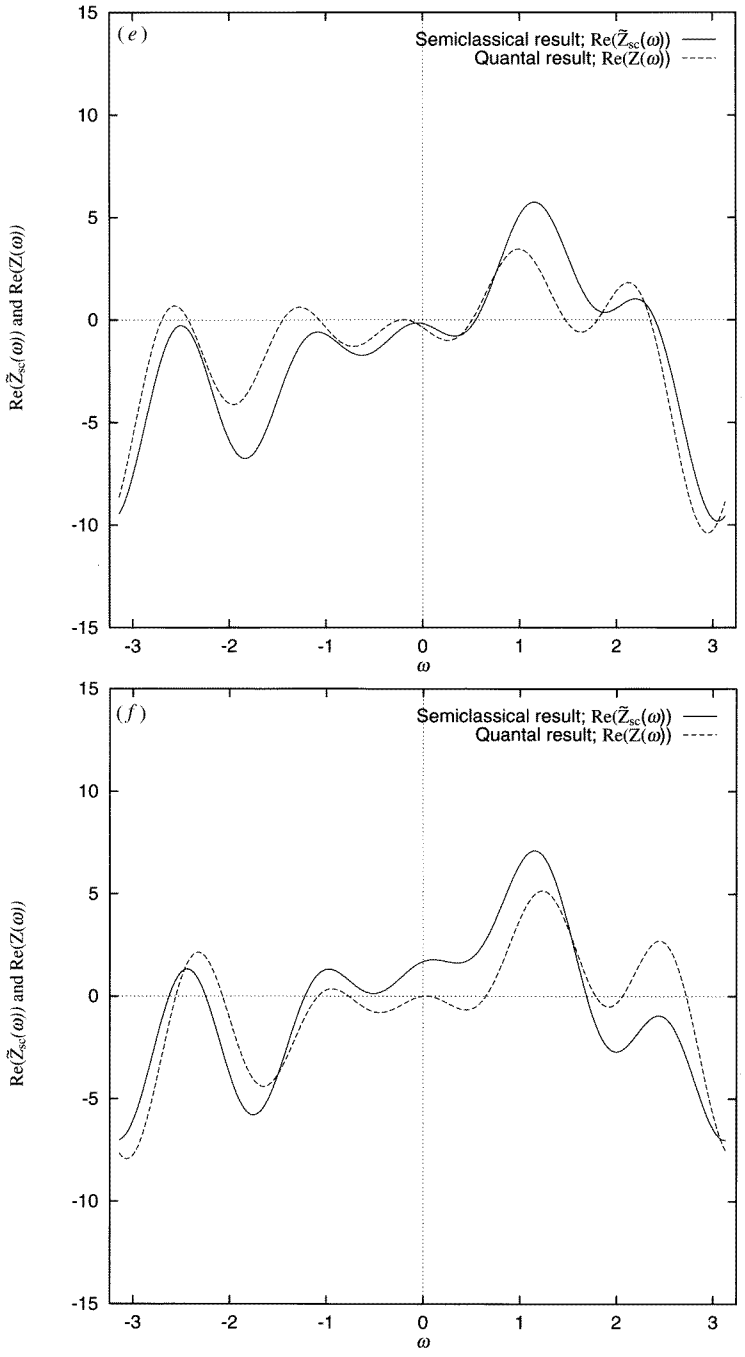

Figure 6. (Continued)

4. The diffractive contributions

In this section we investigate the trace carefully. Applying the Poisson summation formula to the trace of equation (8), we rewrite the trace $\mathrm{Tr}(\hat{U}^T)$:

$$\mathrm{Tr}(\hat{U}^T) = \mathrm{e}^{-\frac{\mathrm{i}\pi T}{4}} N^{T/2} \sum_{\{l_i\}=-\infty}^{+\infty} \int_{\mathcal{D}} \mathrm{d}\boldsymbol{x}\, \exp\left[\frac{\mathrm{i}}{\hbar}\phi(\boldsymbol{l};\boldsymbol{x})\right] \tag{23}$$

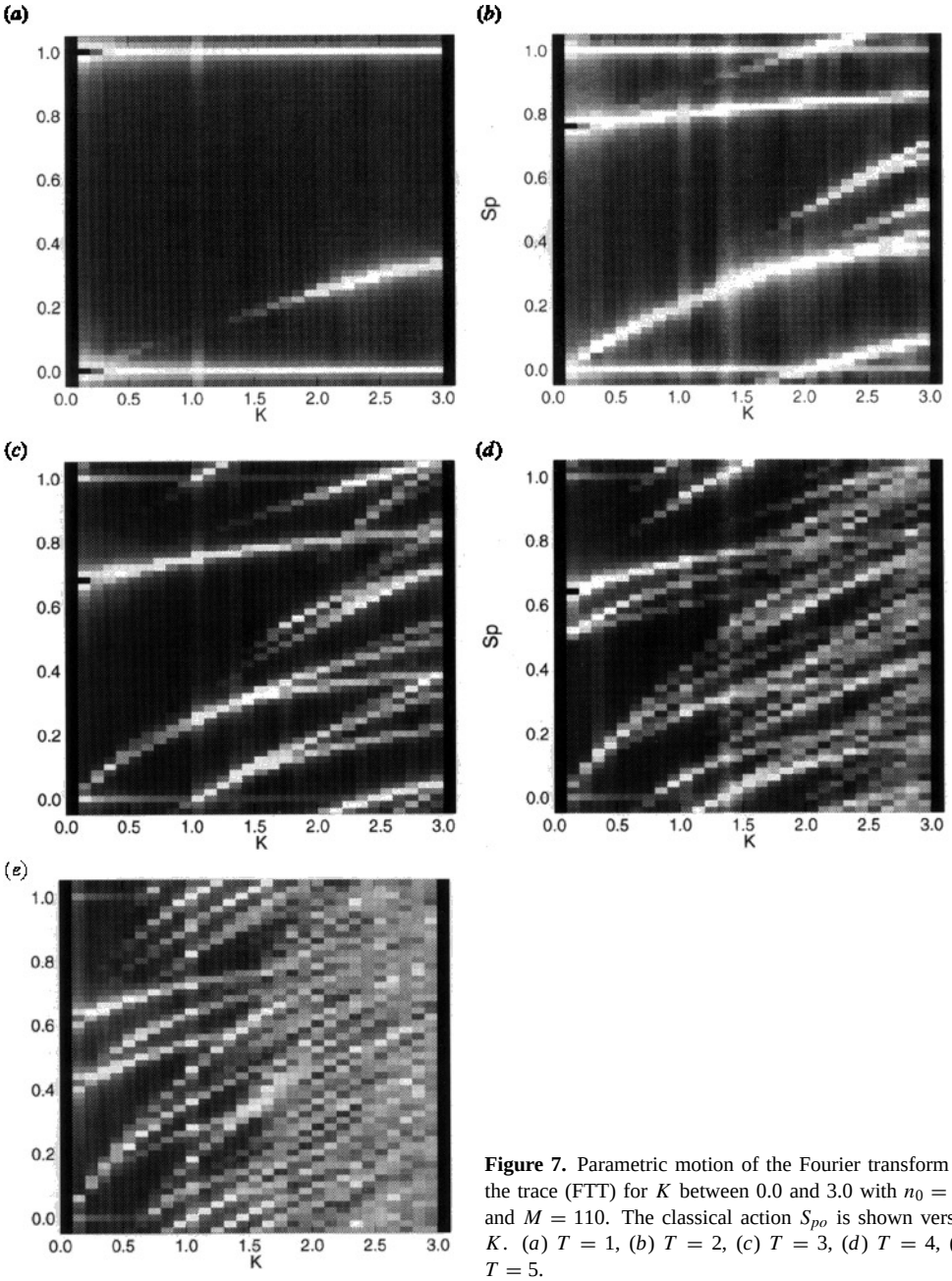

Figure 7. Parametric motion of the Fourier transform of the trace (FTT) for K between 0.0 and 3.0 with $n_0 = 20$ and $M = 110$. The classical action S_{po} is shown versus K. (*a*) $T = 1$, (*b*) $T = 2$, (*c*) $T = 3$, (*d*) $T = 4$, (*e*) $T = 5$.

where $\overline{h} = 1/2\pi N$, $\boldsymbol{x} = (x_1, x_2, \ldots, x_T)$ with $x_i \in [-\frac{1}{2}, \frac{1}{2})$, and $\boldsymbol{l} = (l_1, l_2, \ldots, l_T)$ with $l_i \in \mathbb{Z}$. The phase $\phi(\boldsymbol{l}; \boldsymbol{x})$ is given as

$$\phi(\boldsymbol{l}; \boldsymbol{x}) = \boldsymbol{l} \cdot \boldsymbol{x} + \tfrac{1}{2}\boldsymbol{x}^{\top} \cdot \mathbf{A} \cdot \boldsymbol{x} \tag{24}$$

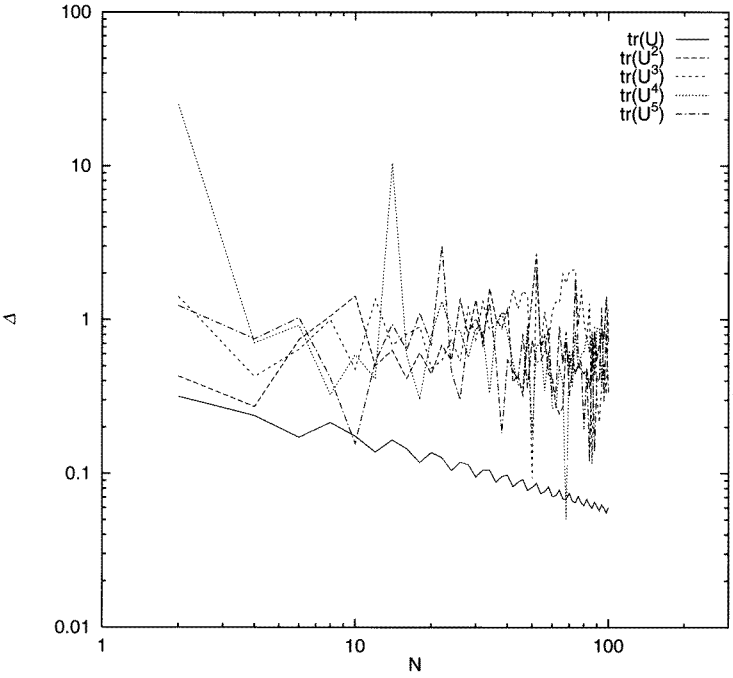

Figure 8. The $\bar{h}$-dependence of the deviation of the semiclassical trace from the exact trace, $\Delta = |\operatorname{Tr}(\hat{U}^T)_{\mathrm{q}} - \operatorname{Tr}(\hat{U}^T)_{\mathrm{sc}}|/|\operatorname{Tr}(\hat{U}^T)_{\mathrm{q}}|$. $N = 1/2\pi\bar{h}$ is the matrix size. The results for periods $T = 1, 2, \ldots, 5$ are depicted for the system parameter $K = 1.3$.

where $\mathbf{A}$ is the matrix

$$\mathbf{A} = \begin{pmatrix} K+2 & -1 & 0 & \cdots & 0 & -1 \\ -1 & K+2 & -1 & & & 0 \\ 0 & -1 & K+2 & \ddots & & \vdots \\ \vdots & & \ddots & \ddots & -1 & 0 \\ 0 & & & -1 & K+2 & -1 \\ -1 & 0 & \cdots & 0 & -1 & K+2 \end{pmatrix}. \tag{25}$$

The range of integration in equation (23) is $\mathcal{D} = [-\frac{1}{2}, \frac{1}{2})^T$. The leading-order contribution to the trace is already given in equation (15). The technical details of the derivation of the next-leading-order contribution is given in the appendix. The result is

$$\begin{aligned} \operatorname{Tr}(\hat{U}^T)|_{\mathrm{Diff;SP}} \simeq{}& \frac{T\mathrm{e}^{-\mathrm{i}\pi/4}(2\pi\bar{h})^{1/2}}{2\mathrm{i}\sqrt{|\det(\mathbf{A}')|}} \\ &\times \sum_{\mathrm{Diff;SP}} \left\{ \exp\left[\frac{\mathrm{i}}{\bar{h}}\Phi(\boldsymbol{l}';\boldsymbol{x}'^*)\right] \cot\left[\pi\left(\frac{K+2}{2} - x_2^* - x_T^*\right)\right]\Big|_{\boldsymbol{x}=\boldsymbol{x}^*;x_1=\frac{1}{2}} \right. \\ &\left. + \exp\left[\frac{\mathrm{i}}{\bar{h}}\Phi(\boldsymbol{l}';\boldsymbol{x}'^*)\right] \cot\left[\pi\left(\frac{K+2}{2} + x_2^* + x_T^*\right)\right]\Big|_{\boldsymbol{x}=\boldsymbol{x}^*;x_1=-\frac{1}{2}} \right\} \end{aligned} \tag{26}$$

where the matrix $\mathbf{A}'$ is defined in equation (A3):

$$\Phi(\boldsymbol{l}';\boldsymbol{x}') = \sum_{j=2}^{T} l_j x_j + \frac{K+2}{2}\sum_{j=2}^{T} x_j^2 - 2\sum_{j=2}^{T-1} x_j x_{j+1} + \frac{K+2}{8} \pm x_2 \pm x_T \tag{27}$$

and

$$\boldsymbol{x}' = (x_2, x_3, \ldots, x_T) \qquad \boldsymbol{l}' = (l_2, l_3, \ldots, l_T) \tag{28}$$

and the signs $\pm$ correspond to $x_1 = \pm\frac{1}{2}$, respectively. For the actual numerical calculation of the diffractive contribution, the following relation is very useful:

$$\boldsymbol{l}' + \mathbf{A}'\boldsymbol{x}' - \boldsymbol{b}' = \mathbf{0} \tag{29}$$

where $\boldsymbol{b}' = (\pm\frac{1}{2}, 0, \ldots, 0, \pm\frac{1}{2})$. The integers $l_2, \ldots, l_T$ provide a symbolic description for these diffraction orbits. The determinant of the $(T-1)\times(T-1)$ matrix $\mathbf{A}'$ is explicitly evaluated as

$$\det(\mathbf{A}') = \left(\lambda - \frac{1}{\lambda}\right)^{-1}\left(\lambda^T - \frac{1}{\lambda^T}\right) \tag{30}$$

where λ is the largest eigenvalue of the one-step tangent map.

Here we include the diffraction effect of order $\mathcal{O}(\overline{h}^{1/2})$ derived here. To see whether the inclusion of this term improves the approximation, the FTT is shown in figure 9 for $K = 1.3$ and $T = 1, 2, \ldots, 5$. The vertical axis represents the absolute value of the difference between the quantum exact result $A(S; M, n_0, T)_{\mathrm{q}}$, the leading-order approximation $A(S; M, n_0, T)_{1\mathrm{st}}$, and second-order approximation (i.e. the diffractive contribution) $A(S; M, n_0, T)_{2\mathrm{nd}}$ of the FTT spectrum. The horizontal axis is the action shown as $2S_{po} \bmod 1$, because we put $N =$ even, for numerical convenience. The vertical solid lines are located at the action values corresponding to the real prime periodic orbits. We do not show the repetitions of the prime periodic orbits. As we can see, however, there is no improvement for the higher $\mathrm{Tr}(\hat{U}^T)$. In particular, the contribution for $T = 5$ seems to be divergent. We have also tried other values of $N = 1/2\pi\overline{h}$ and K, with qualitatively similar results. The reason for the failure discussed above is that the cotangent in equation (26) causes a divergence. This cotangent diverges when the argument approaches integer multiples of π, namely at the bifurcation points. In order that the series should be meaningful, we have to avoid the neighbourhoods of the bifurcation points. The width of these dangerous zones can be roughly estimated as follows. In order to avoid the dangerous zone, the magnitude of the cotangent should be less than 1. Therefore, the width ΔK of the dangerous zone is given by the condition

$$\left|\overline{h}^{1/2}\cot\left(\pi\left(\frac{K_{\mathrm{bf}} + \frac{\Delta K}{2} + 2}{2} \pm x_2^* \pm x_T^*\right)\right)\right| \approx 1 \tag{31}$$

where K_{bf} is the bifurcation point. However, as shown in figure 3 the bifurcations of the periodic orbits occur successively, and the dangerous zones around the different bifurcations overlap. Thus there is no safety zone for this asymptotic series.

Consider next the semiclassical limit $\overline{h} \to 0$. In this limit, in order to quantize the sawtooth map, longer periodic orbits up to period $[N/2] = [1/4\pi\overline{h}]$ are required. As a result, the number of periodic orbits needed increases exponentially. The longer periodic orbits form the smaller steps in figure 3. Consequently, with the increased number of the periodic orbits, these steps become finer and the intervals between steps become narrower. On the other hand, the dangerous zones also become narrower, because these widths are

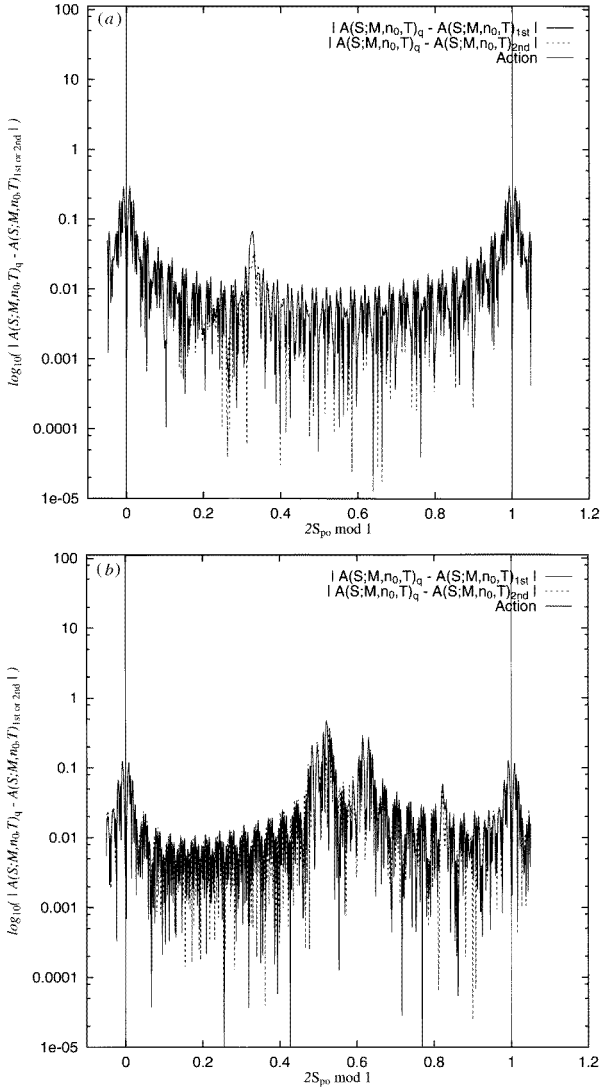

Figure 9. The differences of the FTT spectrum between the exact quantum result and the leading-order approximation and between the exact quantum result and the second-order approximation for $K = 1.3$. (*a*) $T = 1$, (*b*) $T = 2$, (*c*) $T = 3$, (*d*) $T = 4$, (*e*) $T = 5$. The vertical axis represents the absolute value of the difference between the quantum exact result and the leading (second-order) approximation, shown on a logarithmic. The horizontal axis represents the action as $2S_{po} \bmod 1$. The plot for the leading-order (second-order) approximation is in the full (broken) curve. The vertical full line indicates the action of the real prime periodic orbit at $2S_{po} \bmod 1$. (Note that the repetitions of the prime periodic orbits are excluded.). Here we only consider $N = 1/2\pi\bar{h} =$ even.

controlled by $\bar{h}$. In this limit, we do not know which effect dominates at different values of $\bar{h}$. This remains an open problem.

The appearance of the cotangent function in equation (31) originates from the use of integration by parts for the integral (23) and the sum over l_i in equation (23). Integration

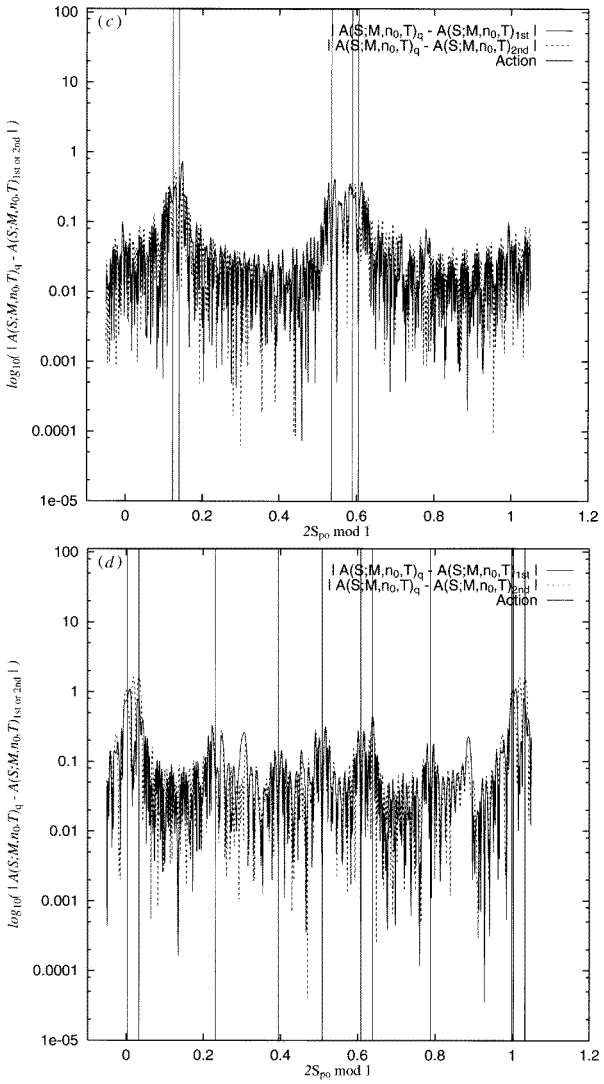

Figure 9. (Continued)

by parts is the most primitive method for obtaining asymptotic series†. In order to improve the accuracy in the neighbourhoods of the bifurcation points, we can use the uniform approximation. For $\mathrm{Tr}(\hat{U})$, our problem is reduced to the evaluation of the following type of integrals:

$$I = \int_0^\infty \mathrm{d}u \, \exp\left[\mathrm{i}\lambda\left(\frac{u^2}{2} - \alpha u\right)\right] \tag{32}$$

† There is another procedure for obtaining the asymptotic series. That is the Euler–Maclaurin sum formula [35]. However, the Euler–Maclaurin sum formula does not have the semiclassical picture and the extension to the multiple sum is unknown.

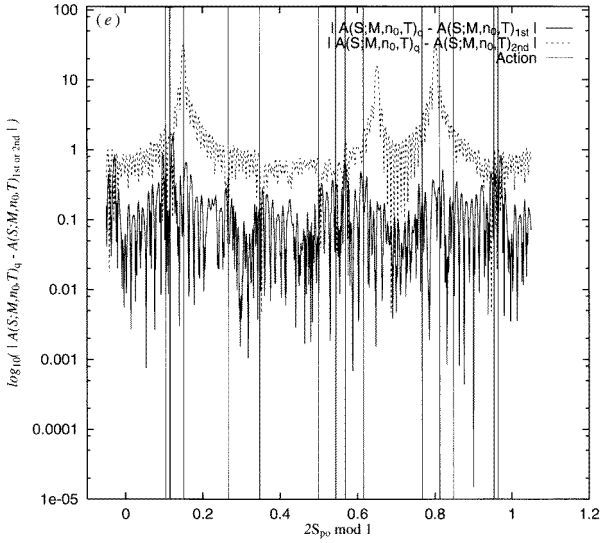

Figure 9. (Continued)

where λ is a large parameter, and α is a real number. This integral is nothing but the canonical function in the standard uniform approximation [29]. More precisely, it is just a variant of the Fresnel integral. This implies that the contribution from each real and diffrative periodic orbit is evaluated *exactly* by the leading order of the uniform approximation. Then, there is no higher-order corrections in this case. However, we have to sum up an infinite number of integrals of the type of equation (32). For $\mathrm{Tr}(\hat{U}^T)$, $T \geqslant 2$, unfortunately, the procedure of the uniform approximation is unknown.

5. Summary

In this paper, we revised the semiclassical quantization of the sawtooth map from the viewpoint of the higher-order contributions beyond the leading order. The numerical calculation including the diffrative contributions shows that for non-integer K, the usual semiclassical theory does not mimic quantum theory, even when we include the diffractive contribution. In particular, the semiclassical zeta function does not cross real zero axis in some cases. The failure seems to be due to two factors: (1) the large value of $\overline{h}$ in the deep quantum regime; (2) the bifurcation of periodic orbits. The numerical observations suggest that the immediate release of the level degeneracies and the bifurcation of periodic orbits are related each other. Consequently, we have explicitly demonstrated a new type of obstacle to the semiclassical theory of quantized chaotic systems. However, this is not a discouraging result. Rather, it is an exciting result that it indicates the desirability of investigating the relations among the different contributions from the periodic orbits (all saddle-point contributions). Further research is clearly required.

Recently, in [37], the accuracy of the trace $\mathrm{Tr}(\hat{U})$ for sawtooth maps was very carefully checked within the leading-order approximation. The error of $\mathrm{Tr}^{\mathrm{sc}}(\hat{U})$ decreases for very large N. However, although individual trace may be well approximated by the leading-order terms, the totality of the underlying chaotic dynamics is very important for the semiclassical

evaluation of eigenvalues, as shown in the present paper. Unfortunately, even though the sawtooth map is very simple, the semiclassical enumeration of eigenvalues in such a large-N regime is practically impossible. Another route for further investigation is needed. The number-theoretical method may be efficient as it succeeded for the Arnold cat map.

Next we compare the results of the present investigation with the case of the quantized baker map, which also has diffraction effects, but no bifurcations. The order of the next-leading contribution is $\mathcal{O}(\overline{h}^{\frac{1}{2}})$, the same as in our case [31, 32]. The explicit formula was derived and applied for the evaluation of the trace in [32]. The authors of [32] pick up the terms which include the stationary point, from an infinite number of integrals which comes from the use of the Poisson sum formula, and explicitly evaluate these terms. This procedure can be also applied for the sawtooth map and will get good accuracy, because the remaining terms give an exponentially small contribution (but their number is infinite). However, the terms which these authors evaluated, are not ordered in $\overline{h}$. This is a difficult point of the diffraction problem. The anomalous behaviour, which comes from the diffraction effect of $\mathcal{O}(\overline{h}^{1/2})$ were observed in the time evolution [33] and discussed for the case of the semiclassical form factor in [34]. Since the order of the next-order contribution is essential for these arguments, the similar behaviour may be expected for the quantized sawtooth map.

Finally, to obtain a full understanding of the universal properties (such as level repulsion) of quantized chaotic systems via the corresponding classical dynamics, one needs a simple and analytically treatable model and a mathematical tool to handle the whole asymptotic series. For the latter, elaborate methods like hyperasymptotics [36] would be essential.

Acknowledgments

The author would like to thank K Kitahara and G Nicolis for continuous encouragement and support and P Gaspard for daily discussions. The author is also grateful to S Adachi, D Alonso for useful discussions, to J P Keating for informing him of [32], and to P A Rikvold for carefully reading the manuscript. For numerical diagonalizations, REISPACK was used [38]. This work was supported by the Grants-in-Aid for Scientific Research from the Ministry of Education, Science and Culture of Japan and a fellowship of the French community of Belgium.

Appendix. Derivation of the diffractive contribution

A.1. $\mathrm{Tr}(\hat{U}^T)$ *for arbitrary* $T \geqslant 3$

By applying results on multiple integrals of the Fourier type [29], we can evaluate the higher-order contributions to $\mathrm{Tr}(\hat{U}^T)$. First, we rewrite the T-dimensional integral into the $(T-1)$-dimensional integral, using the divergence theorem:

$$\sum_{\{l_i\}=-\infty}^{+\infty} \int_{\mathcal{D}} \exp\left[\frac{\mathrm{i}}{\overline{h}}\phi(\boldsymbol{l};\boldsymbol{x})\right] \mathrm{d}\boldsymbol{x} = \frac{\overline{h}}{\mathrm{i}} \sum_{\{l_i\}=-\infty}^{+\infty} \int_{\partial\mathcal{D}} \mathrm{d}\Sigma \, \exp\left[\frac{\mathrm{i}}{\overline{h}}\phi(\boldsymbol{l};\boldsymbol{x})\right] \frac{\boldsymbol{N}\cdot\nabla\phi}{|\nabla\phi|^2}. \tag{A1}$$

Carrying out the stationary-phase approximation, we obtain

$$\sum_{\{l_i\}=-\infty}^{+\infty} \int_{\mathcal{D}} \exp\left[\frac{\mathrm{i}}{\overline{h}}\phi(\boldsymbol{l};\boldsymbol{x})\right] \mathrm{d}\boldsymbol{x} \cong \frac{\overline{h}}{\mathrm{i}} \sum_{\{l_i\}=-\infty}^{+\infty} \sum_{\mathrm{SP}} \exp\left[\frac{\mathrm{i}}{\overline{h}}\phi(\boldsymbol{l};\boldsymbol{x}^*)\right] \frac{\mathrm{sgn}[\boldsymbol{N}\cdot\nabla\phi]}{|\nabla\phi|} \frac{(2\pi\overline{h})^{\frac{T-1}{2}}}{\sqrt{|\det(\mathbf{A}')|}} \tag{A2}$$

where the sum is taken over the contributions of the stationary points and $\mathbf{A}'$ is a $(T-1)\times(T-1)$ real symmetric tridiagonal matrix:

$$\mathbf{A}' = \begin{pmatrix} K+2 & -1 & 0 & \cdots & 0 & 0 \\ -1 & K+2 & -1 & & & 0 \\ 0 & -1 & K+2 & \ddots & & \vdots \\ \vdots & & \ddots & \ddots & -1 & 0 \\ 0 & & & -1 & K+2 & -1 \\ 0 & 0 & \cdots & 0 & -1 & K+2 \end{pmatrix}. \tag{A3}$$

The domain $\mathcal{D}$ is a T-dimensional hypercube. Thus, $\mathcal{D}$ has $2T$ $(T-1)$-dimensional hypercubes as its surface. There are $2T$ different locations of the stationary points on $\partial\mathcal{D}$. However, by considering each case, we find that there are, essentially, only two different cases, because $\phi(\boldsymbol{l};\boldsymbol{x})$ is symmetric with respect to $\boldsymbol{l}$ and $\boldsymbol{x}$. These two cases correspond to $x_k = \pm\frac{1}{2}$ in each direction x_k. Therefore, we only specify the location on one pair of faces of the T-dimensional hyperplain $\mathcal{D}$: $x_1 = \pm\frac{1}{2}$. The corresponding stationary phase condition gives the equations for the stationary phase point:

$$\begin{aligned} &l_1 + (K+2)(\pm\tfrac{1}{2}) - x_2 - x_T \neq 0 \\ &l_2 + (K+2)x_2 - x_3 - (\pm\tfrac{1}{2}) = 0 \\ &l_3 + (K+2)x_3 - x_4 - x_2 = 0 \\ &\qquad\vdots \\ &l_{T-1} + (K+2)x_{T-1} - x_T - x_{T-2} = 0 \\ &l_T + (K+2)x_T - (\pm\tfrac{1}{2}) - x_{T-1} = 0. \end{aligned} \tag{A4}$$

Here the first line is due to the discontinuity at the boundary of the configuration space. From this stationary phase condition, we obtain the physical meaning of the corresponding classical orbit in the sense used by Keller [10]: the corresponding orbit eventually reaches one of the boundaries at $x = \pm\frac{1}{2}$. As shown below (equation (A6)), at the boundary, the momentum is shifted by an amount

$$\cdots \to \begin{bmatrix} x_T \\ p_T \end{bmatrix} \to \begin{bmatrix} x_1 = \pm\frac{1}{2} \\ p_1 \end{bmatrix} \to \begin{bmatrix} x_2 \\ p_{2,\alpha} \end{bmatrix} \uparrow \text{Discontinuous} \downarrow \begin{bmatrix} x_2 \\ p_{2,\beta} y \end{bmatrix} \to \begin{bmatrix} x_3 \\ p_3 \end{bmatrix} \to \cdots \tag{A5}$$

where $p_{2,\alpha} \neq p_{2,\beta}$. The resulting expression for this contribution is

$$\begin{aligned} \mathrm{Tr}(\hat{U}^T)|_{\mathrm{Diff;SP}} \simeq{}& \frac{T\mathrm{e}^{-\mathrm{i}\pi/4}(2\pi\bar{h})^{-1/2}\bar{h}}{\mathrm{i}\sqrt{|\det(\mathbf{A}')|}} \sum_{\mathrm{Diff;SP}} \sum_{l_1=-\infty}^{+\infty} \sum_{l_2,l_3,\ldots,l_T=-\infty}^{\infty} \\ &\times \left\{ \exp\left[\frac{\mathrm{i}}{\bar{h}}\phi(\boldsymbol{l};\boldsymbol{x}^*)\right] \frac{\mathrm{sgn}[\boldsymbol{N}\cdot\nabla\phi]}{|l_1 + \frac{K+2}{2} - x_2^* - x_T^*|}\bigg|_{\boldsymbol{x}=\boldsymbol{x}^*;x_1=\frac{1}{2}} \right. \\ &\left. + \exp\left[\frac{\mathrm{i}}{\bar{h}}\phi(\boldsymbol{l};\boldsymbol{x}^*)\right] \frac{\mathrm{sgn}[\boldsymbol{N}\cdot\nabla\phi]}{|l_1 - \frac{K+2}{2} - x_2^* - x_T^*|}\bigg|_{\boldsymbol{x}=\boldsymbol{x}^*;x_1=-\frac{1}{2}} \right\}. \end{aligned} \tag{A6}$$

The amplitude factor in equation (A6) is related to the difference between the momenta. This is very similar to the diffraction orbits for the wedge, as discussed by Keller [10]. Actually, the diffraction coefficient for the wedge which is the amplitude factor for the diffraction orbit, corresponds to the angle difference between the incoming and the outgoing directions at the wedge (for a nice re-derivation, see [30]). Finally, using the following relation

$$\sum_{n=-\infty}^{+\infty} \frac{1}{n+\alpha} = \pi \cot(\pi\alpha) \qquad (\alpha \text{ is not integer.}) \tag{A7}$$

Equation (26) is immediately obtained.

A.2 $Tr(\hat{U})$

For this case, the exact quantum trace is reduced to

$$\begin{aligned} \mathrm{Tr}(\hat{U}) &= \frac{\mathrm{e}^{-\mathrm{i}\pi/4}}{\sqrt{N}} \sum_{n=-N/2}^{N/2-1} \exp\left(\frac{\mathrm{i}\pi K}{N} n^2\right) \\ &= \mathrm{e}^{-\mathrm{i}\pi/4}\sqrt{N} \sum_{l=-\infty}^{+\infty} \int_{-\frac{1}{2}+\epsilon}^{+\frac{1}{2}-\epsilon} \mathrm{d}x \ \exp[\mathrm{i}\pi N(Kx^2 - 2lx)]. \end{aligned} \tag{A8}$$

In the second line, we here used the Poisson sum formula. First, if, for a certain value of l, there is a stationary phase point x^* in $[-\frac{1}{2}, \frac{1}{2})$, then we divide the integral into three pieces:

$$\int_{-\frac{1}{2}+\epsilon}^{\frac{1}{2}-\epsilon} = \int_{-\infty}^{+\infty} - \int_{-\infty}^{-\frac{1}{2}-\epsilon} - \int_{+\frac{1}{2}+\epsilon}^{+\infty}. \tag{A9}$$

The first term on the r.h.s. can be exactly evaluated by the usual stationary approximation. The second and third terms which arise from the edge of the interval of integration can be evaluated by successive applications of integration by parts. For the case that there is no stationary point in $[-\frac{1}{2}, \frac{1}{2})$, the contribution can be evaluated by integration by parts in the same way. Summing up the stationary and edge contributions, we obtain

$\mathrm{Tr}(\hat{U}) \simeq$ (Contribution from stationary points)

$$+\mathrm{e}^{\mathrm{i}K/\hbar 8 - \mathrm{i}\pi/4} \frac{(2\pi\hbar)^{1/2}}{\pi} \sum_{n=0}^{+\infty} \frac{(2\hbar K)^n (n-\frac{1}{2})!}{\mathrm{i}^{n+1}} \mathcal{F}_{2n+1}\left(\frac{K}{2}\right) \tag{A10}$$

where

$$\mathcal{F}_k(x) = \sum_{l=-\infty}^{+\infty} \frac{1}{(x+l)^k}. \tag{A11}$$

Several $\mathcal{F}_k(x)$'s are given by

$$\mathcal{F}_1(x) = \pi X \tag{A12}$$

$$\mathcal{F}_3(x) = \pi^3 X(1 + X^2) \tag{A13}$$

$$\mathcal{F}_5(x) = \pi^5 X(\tfrac{2}{3} + \tfrac{5}{3}X^2 + X^4) \tag{A14}$$

$$\mathcal{F}_7(x) = \pi^7 X(\tfrac{17}{45} + \tfrac{77}{45}X^2 + \tfrac{7}{3}X^4 + X^6) \tag{A15}$$

$$\mathcal{F}_9(x) = \pi^9 X(\tfrac{62}{315} + \tfrac{88}{63}X^2 + \tfrac{16}{5}X^4 + 3X^6 + X^8) \tag{A16}$$

where

$$X = \cot(\pi x). \tag{A17}$$

When $K(>0)$ is an even integer, $\mathcal{F}_{2n+1}(K/2)$, this contribution diverges. This corresponds to the bifurcation of the fixed points.

A.3. $Tr(\hat{U}^2)$

A.3.1. Contribution from the stationary points on $\partial\mathcal{D}$. Applying the result in section A.1, we obtain the contribution from the stationary points on $\partial\mathcal{D}$ as follows:

$$\begin{aligned}\mathrm{Tr}(\hat{U}^2)|_{\mathrm{Diff;SP}} \simeq & -\exp\left(-\frac{\mathrm{i}\pi}{4}\right)\left(\frac{2\pi\bar{h}}{K+2}\right)^{1/2} \\ & \times\Bigg\{\sum_{-\frac{K}{2}<l_2\leqslant\frac{K}{2}+2}\cot\left[\pi\left(\frac{K+2}{2}-\frac{2(1-l_2)}{K+2}\right)\right] \\ & \times\exp\left[\frac{\mathrm{i}}{\bar{h}}\left(\frac{K+2}{8}-\frac{(1-l_2)^2}{2(K+2)}\right)\right] \\ & +\sum_{-\frac{K}{2}-2\leqslant l_2<\frac{K}{2}}\cot\left[\pi\left(\frac{K+2}{2}+\frac{2(1+l_2)}{K+2}\right)\right] \\ & \times\exp\left[\frac{\mathrm{i}}{\bar{h}}\left(\frac{K+2}{8}-\frac{(1+l_2)^2}{2(K+2)}\right)\right]\Bigg\}. \end{aligned} \tag{A18}$$

A.3.2. Contribution from the critical points on $\partial\mathcal{D}$

$$\mathrm{Tr}(\hat{U}^2)|_{\mathrm{Diff;Corner}} \simeq (2\pi\bar{h})\exp\left(\frac{\mathrm{i}}{\bar{h}}\frac{K}{4}\right)\left(\cot\left(\frac{\pi K}{2}\right)\right)^2. \tag{A19}$$

When $K(>0)$ is an even integer, the r.h.s. diverges. Since the action $K/8$ in equation (A19) is twice as large as in equation (A10), the contribution of the action of $\mathrm{Tr}(\hat{U}^2)$ is just the repetition of the action to $\mathrm{Tr}(\hat{U})$.

References

[1] Gutzwiller M C 1970 *J. Math. Phys.* **11** 1791; 1971 *J. Math. Phys.* **12** 343; 1990 *Chaos in Classical and Quantum Mechanics* (Berlin: Springer)

[2] Voros A 1988 *J. Phys. A: Math. Gen.* **21** 685; 1987 *Commun. Math. Phys.* **110** 439
CvitanovićP and Eckhardt B 1989 *Phys. Rev. Lett.* **63** 823

[3] Berry M V and Keating J P 1990 *J. Phys. A: Math. Gen.* **23** 4839; 1992 *Proc. R. Soc.* A **437** 151
Keating J P 1992 *Proc. R. Soc.* A **436** 99

[4] Franz W and Deppermann K 1952 *Ann. Phys.* **10** 361; 1954 *Ann. Phys.* **14** 253
Franz W 1954 *Z. Phys.* A **9** 705

[5] Oberhettinger F 1958 *J. Res. Natl Bur. Stand.* **61** 343; Oberhettinger 1954 *Commun. Pure Appl. Math.* **7** 551

[6] Shimizu Y and Shudo A 1994 *Prog. Theor. Phys. Suppl.* **116** 267

[7] Sano M M 1992 *J. Phys. A: Math. Gen.* **27** 4791

[8] Sano M M 1995 *Proc. Int. Conf. Dynamical Systems and Chaos (Tokyo Metropolitan University, 1994) (Physics)* vol 2 (Singapore: World Scientific) p 471

[9] Sano M M 1995 *PhD Thesis* Tokyo Institute of Technology, unpublished

[10] Keller J B 1962 *J. Opt. Soc. Am.* **52** 116; 1958 *Geometrical Theory of Diffraction* (Providence, RI: American Mathematical Society) p 27

[11] Landau L D and Lifshitz E M 1977 *Landau and Lifshitz, Course of Theoretical Physics Vol 3, Quantum Mechanics (Non-relativistic Theory)* 3rd edn (Oxford: Pergamon)

[12] van der Veldet R, Vassen W and Hagervorst W 1993 *Europhys. Lett.* **21** 903

[13] Shudo A and Ikeda K 1994 *Prog. Theor. Phys. Suppl.* **116** 283; 1995 *Phys. Rev. Lett.* **74** 682; 1996 *Phys. Rev. Lett.* **76** 4151

[14] Gaspard P and Alonso D 1993 *Phys. Rev.* A **4** R3468
Alonso D and Gaspard P 1993 *Chaos* **3** 601 (erratum 1994 *Chaos* **4** 105)
Gaspard P 1994 *Prog. Theor. Phys. Suppl.* **116** 59

[15] Hannay J and Berry M V 1980 *Physica* **1D** 267

[16] Keating J P 1991 *Nonlinearity* **4** 277, 309
[17] Percival I and Vivaldi F 1987 *Physica* **27D** 373; 1987 *Physica* **25D** 105
Bird N and Vivaldi F 1988 *Physica* **30D** 164
Murray N W, Chen Q, Dana I, Meiss J D and Percival I C 1990 *Physica* **46D** 217
Vivaldi F 1987 *Proc. R. Soc.* A **413** 97
Bartucelli M and Vivaldi F 1989 *Physica* **39D** 194
Chen Q and Meiss J D 1989 *Nonlinearity* **2** 347
[18] Lakshminarayan A and Balazs M L 1993 On the quantum cat and sawtooth maps—return to generic behaviour *Preprint*
Lakshminarayan A 1994 *Phys. Lett.* **192A** 345
[19] Basiloi de Matos M and Ozorio de Almeida A M 1995 *Ann. Phys.* **237** 46
[20] Boasman P A and Keating J P 1995 *Proc. R. Soc.* A **449** 629
[21] Arnold V I and Avez A 1967 *Problème ergodiques de la méchanique classique* (Tauthier-Villars)
[22] Adler R L and Weiss B 1970 *Similarity of Automorphisms of the Torus (Memoirs of the American Mathematical Society 98)* (Providence, RI: American Mathematical Society)
[23] Gaspari G 1994 *Physica* **73D** 352
[24] Chernov N I 1992 *J. Stat. Phys.* **69** 111
[25] Smilansky U 1993 *Nucl. Phys.* A **560** 57
[26] Lebœuf P and Mouchet A 1995 *Phys. Rev. Lett.* **73** 1360
[27] Voros A 1983 *Ann. Inst. H. Poincaré* **39** 9
[28] Hannay J H and Ozorio de Almeida A M 1984 *J. Phys. A: Math. Gen.* **17** 3429
[29] Bleistein N and Handelsman R A 1986 *Asymptotic Expansions of Integrals* (New York: Dover)
[30] Dewitt-Morette C, Low S G, Schulman L S and Shiekh A Y 1986 *Found. Phys.* **16** 311
[31] Saraceno M and Voros A 1994 *Physica* **79D** 206
[32] da Luz M G E and Ozorio de Almeida A M 1995 *Nonlinearity* **8** 43
[33] Dittes F-M, Doron E and Smilansky U 1994 *Phys. Rev.* E **49** R963
[34] Keating J P 1994 *J. Phys. A: Math. Gen.* **27** 6605
[35] de Bruijn N G 1981 *Asymptotic Methods in Analysis* (New York: Dover)
[36] Berry M V 1989 *Proc. R. Soc.* A **422** 7
Berry M V and Howls C J 1990 *Proc. R. Soc.* A **430** 653; 1991 *Proc. R. Soc.* A **434** 657
[37] Lakshminarayan A Accuracy of trace formulas *Paramana, J. Phys.* submitted (special issue on nonlinearity and chaos in physical sciences) *Preprint* chao-dyn/9606005
[38] Adachi S 1994 REISPACK which is a remote diagonalization package on workstations. REISPACK was written by S Adachi